



# Using derived-stereo imagery to map macroscale ice-flow features

H. Arnold<sup>1, a</sup>, and A.S. Hickin<sup>1</sup>

<sup>1</sup>British Columbia Geological Survey, Ministry of Energy and Mines, Victoria, BC, V8W 9N3

<sup>a</sup>corresponding author: Holly.E.Arnold@gov.bc.ca

Recommended citation: Arnold, H., and Hickin, A.S., 2017. Using derived-stereo imagery to map macroscale ice-flow features. In: Geological Fieldwork 2016, British Columbia Ministry of Energy and Mines, British Columbia Geological Survey Paper 2017-1, pp. 215-229.

---

## Abstract

Understanding the extent, flow paths, and history of glaciers and ice sheets comes from interpreting landforms, some of which were created by subglacial processes. Subglacial streamlined landforms, such as crag-and-tails, drumlins, drumlinoids, and flutes (ice-flow features), form parallel to ice flow. Given the cost of fieldwork in remote regions, even the most recent compilations of these landforms in the Canadian Cordillera are incomplete. Derived-stereo imagery provides the ability to incorporate single-frame imagery into traditional stereo airphoto methods to remotely map these features at significantly less cost. A comparison of stereoscopic air photographs and two derived-stereo imagery types (Satellite Pour l'Observation de la Terre and orthomosaics) to map ice-flow features in the Atlin and Liard Plain areas of northern British Columbia indicates that derived-stereo orthomosaics provide government agencies, who can access the orthomosaics at no cost, the best value to map ice-flow features for the British Columbia Geological Survey ice-flow feature compilation. Although derived-stereo SPOT imagery is inferior to airphotos and derived-stereo orthomosaics, it may be adequate for regional ice-flow studies and, freely accessed, may be better suited to the general public.

**Keywords:** Derived-stereoscopic imagery, stereoscopic imagery, subglacial streamlined landforms, ice-flow feature compilation

---

## 1. Introduction

The Cordilleran Ice Sheet (CIS) refers to the mass of mountain ice caps and interconnected valley and piedmont glaciers that occupied western Canada, Alaska, Washington, Idaho, and Montana during major Quaternary glaciations (Jackson and Clague, 1991). The CIS formed and decayed several times, expanding from topographically controlled alpine glaciers that coalesced and reached sufficient thicknesses to flow independent of topography (Clague, 1989; Fulton, 1991; Jackson and Clague, 1991; Stumpf et al., 2000; Clague and Ward, 2011). Ice-flow landforms and ice sheet models indicate that ice in the interior of British Columbia was thick enough to flow west, across the Coast Mountains and onto the continental shelf, and east, across the Rocky Mountains onto the Canadian Interior Plains (Clague, 1989; Fig. 1). Understanding the extent, flow pathways, and history of the most recent CIS (Late Wisconsinan; ~22-10 ka; almost equivalent to marine isotopic stage 2) comes from interpreting landforms, some of which were created by subglacial processes (see Kleman, et al., 1997; Boulton et al., 2001; King et al., 2009; Clark et al., 2012; Stokes et al., 2015). Landforms, such as crag-and-tails, drumlins, drumlinoids, and flutes are streamlined along ice flow directions (referred to as ice-flow features) (Menzies, 1979; Boulton, 1987; Clark, 1993; Evans et al., 2006; Benn and Evans, 2010). Although Ferbey and Arnold, (2013), Ferbey et al. (2013) and Arnold et al. (2016) have compiled such ice-flow features formed in the Canadian Cordillera, mapping is incomplete. For example, the lack of ice-flow features in

large regions (Arnold et al., 2016) may merely reflect gaps in mapping. The British Columbia Geological Survey and the Geological Survey of Canada, under the Geo-mapping for Energy and Minerals (GEM) program, are collaborating to address some of the mapping inadequacies. In this paper, we evaluate a relatively inexpensive approach that uses small-scale imagery to map macroscale ice-flow features.

Most maps of ice-flow features in British Columbia have been generated using traditional stereoscopic aerial photography (Ferbey et al., 2013), in which sequential frames have significant overlap (60% along flight; 20-40% across flight; e.g., Aber et al., 2010). This overlap, needed for traditional stereo viewing, demands many images, which makes it expensive to map large areas with gaps in the Cordillera. As an alternative approach, digital derived-stereo imagery takes a single image and combines it with a digital elevation model (DEM) to generate a second offset image (DAT/EM, 2012). The original and generated images are combined using photogrammetric software to display a stereoscopic image (i.e., in 3D; DAT/EM, 2012). Because this approach does not require overlapping images, fewer are needed for regional mapping. Furthermore, fewer images or remote sensing scenes (e.g., Landgrebe, 2003) are needed because satellite imagery and orthomosaics commonly extend across large areas, although the resolution of this imagery is commonly lower than traditional digitized airphotos. Here we evaluate stereoscopic aerial photography and two derived-stereo imagery types (Satellite Pour l'Observation de la Terre or SPOT, and orthomosaics) for

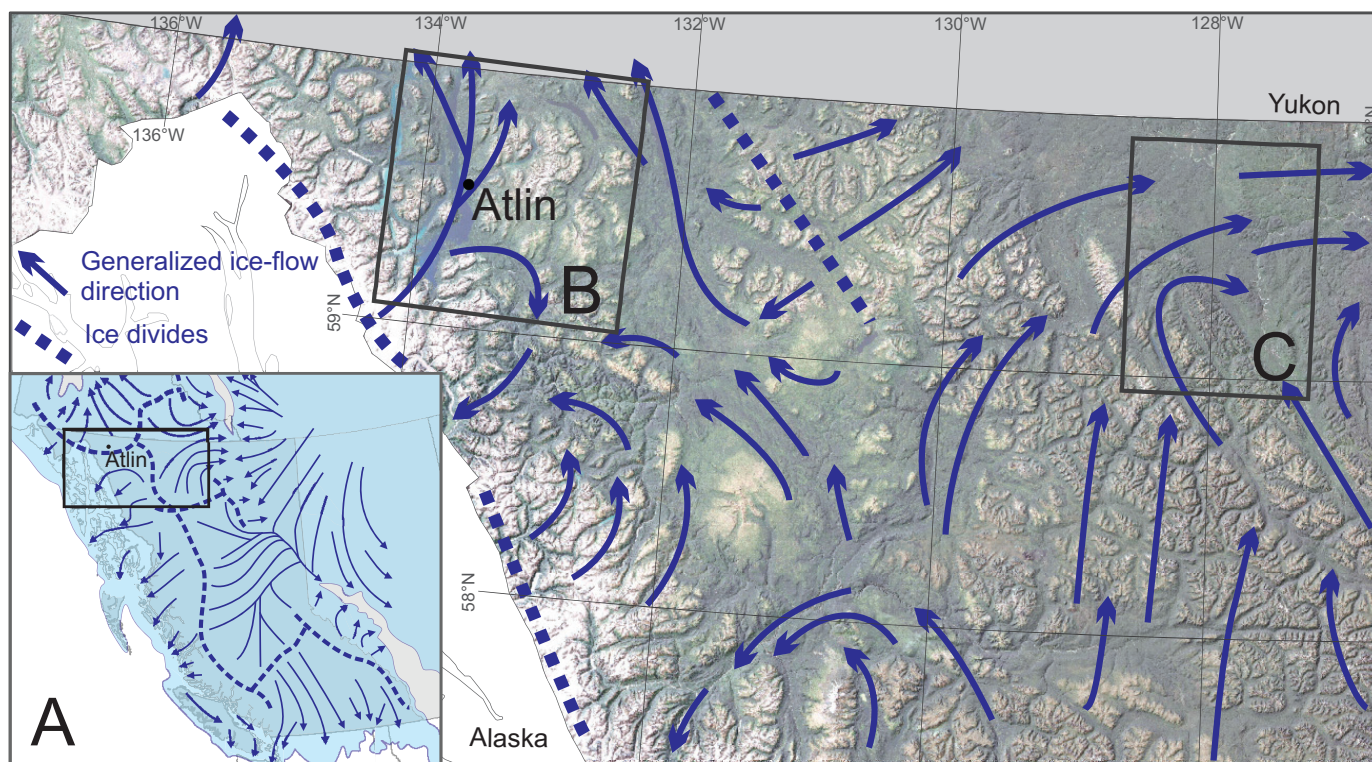


**Fig. 1.** a) Cordilleran ice sheet during the Late Wisconsinan and location of study areas (after Clague and Ward, 2011). Major Late Wisconsinan ice-flow directions in b) the Atlin area and c) the Liard Plain (summarized from Ryder and Maynard, 1991).

mapping ice-flow features in the Atlin and Liard Plain areas of northern British Columbia (Fig. 1).

## 2. Regional setting

The Atlin area was selected because overlapping remote sensing datasets (airphotos and SPOT) and maps depicting ice-flow features (Levson et al., 2003) are available. The Atlin area (Fig. 2a) is in the Teslin Plateau, with its gently sloping uplands and wide valleys. Peaks of the Snowdon, Lina, Johnson, Laurie, and Sloko ranges rise above the plateau surface. To the west, the Tahltan Highlands form the transition from the Teslin Plateau to the Coast Mountains (Holland, 1976). At glacial maximum, ice centres for the northern CIS were most likely over the Coast Mountains west of the Atlin area and in the Skeena Mountains and Stikine Plateau to the south (Figs. 1, 2a; Ryder and Maynard, 1991; Seguinot et al., 2016). Aitken (1959) interpreted that three ice streams flowed through the Atlin area. Accordingly, one flowed northeast from the Coast Mountains, north along Atlin Lake, then branched northwest through the Jones Lake valley (Aitken, 1959; Levson et al., 2003). The second flowed from the south end of Atlin Lake, east through the Pike and O'Donnell valley before deflecting south into the Taku Trench (Figs. 1, 2a). A third ice stream, probably sourced from ice caps in the Stikine Plateau, flowed through the broad valley now occupied by Gladys Lake and Hall Lake (Fig. 2a) and is part of the Teslin ice stream, which can be tracked more than 500 km from Tanzilla River in British Columbia, north into Yukon (Ryder and Maynard, 1991). Major

topographic features have had a profound influence on the ice-flow directions of both ice streams and valley glaciers (Ryder and Maynard, 1991). During deglaciation, topography and local relief likely controlled the flow of valley glaciers sourced in upland areas (Fig. 2a).

The Liard Plain was also selected because overlapping remote sensing datasets and maps depicting ice flow (Gabrielse, 1963) are available. The gently rolling lowlands of the Liard Plain rise in elevation to the southwest into the flat-topped ridges and rounded mountains of the Dease Plateau, southeast of which are the rugged mountains of the Ketchika Ranges (Fig. 2b; Holland, 1976). At glacial maximum, the northern CIS in British Columbia flowed north across the western Liard Plain into the Yukon (Jackson, 1994; Kennedy and Bond, 2004) and east through the Liard Plain to the edge of the Cordilleran deformation front, coalescing with the westward-flowing Laurentide Ice Sheet (Bednarski, 2008; Margold et al., 2013; Huntley et al., 2016; Figs. 1, 2b). In the final stages of deglaciation, ice diminished through active retreat rather than ice stagnation (Margold et al., 2013) and ice sourced in local uplands flowed down valleys and converged with montane glaciers that persisted in major trunk valleys.

## 3. Methods

### 3.1. Stereoscopic and derived-stereo imagery

Advances in 3D digital technology have enabled the transition from mapping using hardcopy aerial photographs to the digital environment. Specialized photogrammetric software is used

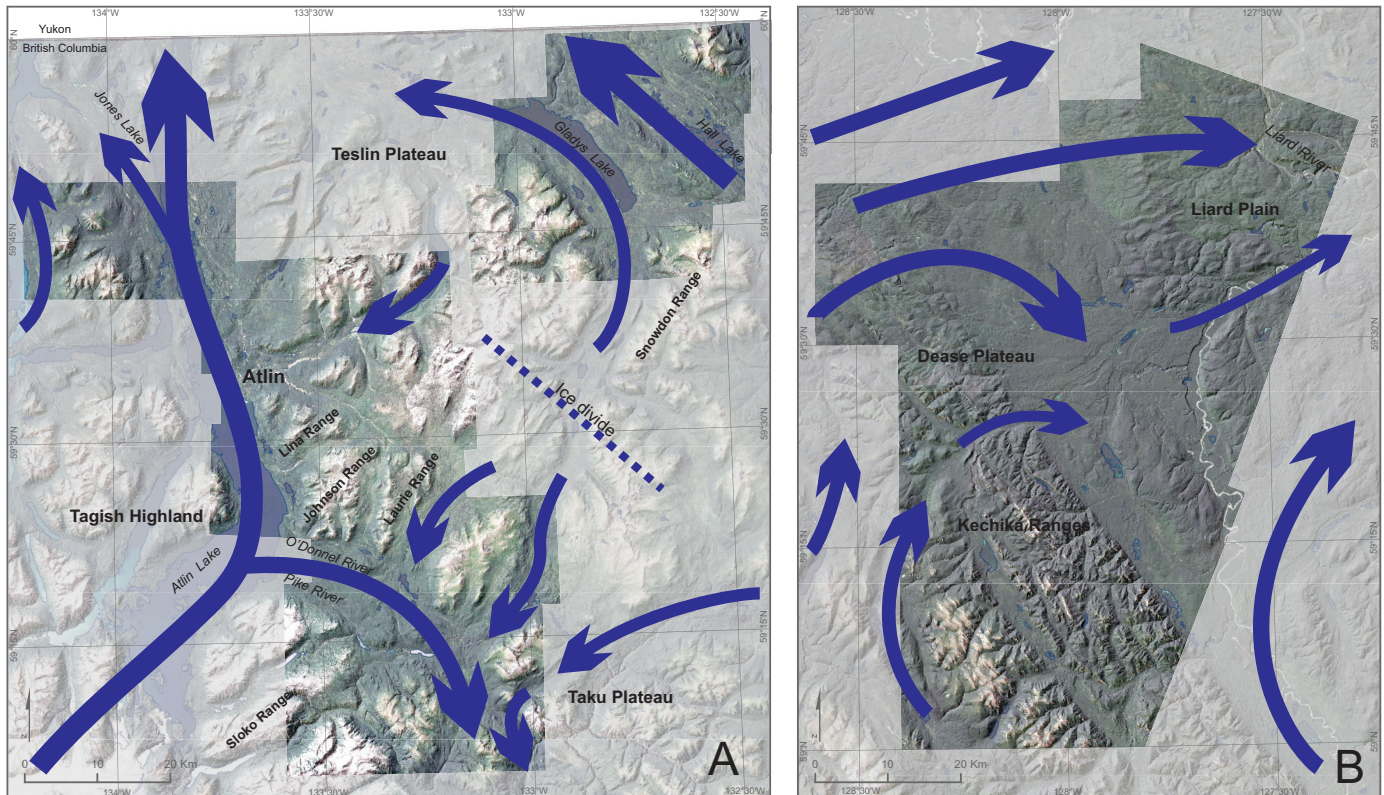


**Fig. 2.** Areas mapped (dark shading). **a)** Atlin area with ice-flow directions during the Late Wisconsinan, summarized from Aitken (1959), Ryder and Maynard (1991), Levson et al. (2003) and Clague and Ward (2011). **b)** Liard Plain area with ice-flow directions during the Late Wisconsinan, summarized from Gabrielse (1963) Jackson and Mackay (1990) Jackson et al. (1991) Ryder and Maynard (1991), and Margold et al. (2013).

to digitize 3D vectors directly into a geographic information system (GIS) and superimpose them on stereo imagery for immediate verification and editing. Stereo imagery (Fig. 3a), such as the airphotos used in this project, can be georeferenced and loaded for use in stereo photogrammetric software. We use SPOT and orthomosaic derived-stereo imagery to evaluate their value for mapping macroscale ice-flow features.

Like traditional stereo-paired airphotos, derived-stereo imagery requires two overlapping images for 3D display. However, unlike stereo-paired photographs, SPOT and orthomosaics are single frames with minimal overlap and must be digitally processed to render an offset image (Fig. 3b). The second, or derived image, is a duplicate of the original and is displaced in the direction of flight by a percent of the DEM resolution. The Shuttle Radar Topography Mission (SRTM) 1 Arc-second DEM was selected to produce derived-stereo imagery (SRTM, 2014). The amount of displacement (shift) selected between the derived and original images is 0.125 of the SRTM DEM resolution (1 Arc-second = ~30 m resolution;  $30 \text{ m} \times 0.125 = 3.75 \text{ m}$  horizontal shift in the direction of flight). The 'new' offset derived image is then draped over the DEM surface to spatially reference each of the pixels in the image. The edges of the new image are no longer straight, but instead pixels are warped to fit onto the DEM. This creates an image with a new perspective which, when combined with the original image, will appear in 3D (Fig. 4). We used DAT

EM's Summit Evolution photogrammetric software to create 3D stereo models. As with imagery flown in stereo, relief in the derived-stereo imagery is exaggerated. This exaggeration is a function of the horizontal offset between the original and derived images and the elevation range in the derived-stereo pair (Fig. 5).

### 3.2. Imagery types

We evaluated three imagery types: 1) traditional stereoscopic panchromatic 1:70,000-scale airphotos; 2) derived-stereo panchromatic SPOT imagery at 10 m resolution; and 3) derived-stereo panchromatic 1:20,000-scale orthomosaics. Fifty-nine digital aerial photographs were purchased from the Government of British Columbia for \$18.50 per photo. The photos were taken in 1987 and 1988 and cover an area of about 4,000 km<sup>2</sup>. A contractor georeferenced each image and digital stereo projects were created using Summit Evolution for \$20 per image (Table 1). Thirteen SPOT images were obtained from the Government of Canada at no cost (SPOT, 2010). Each SPOT image covers about 3,800 km<sup>2</sup> and has overlap of ~15 km west to east and ~5 km north to south (Fig. 3b). The images are from the SPOT 4 and SPOT 5 missions flown between 2005 and 2010. The derived-stereo SPOT imagery was produced by a contractor at a cost of \$20 per image (Table 1). Forty-one orthomosaics were obtained from the Government of British Columbia, at no cost for internal government use; the cost for external users is \$200

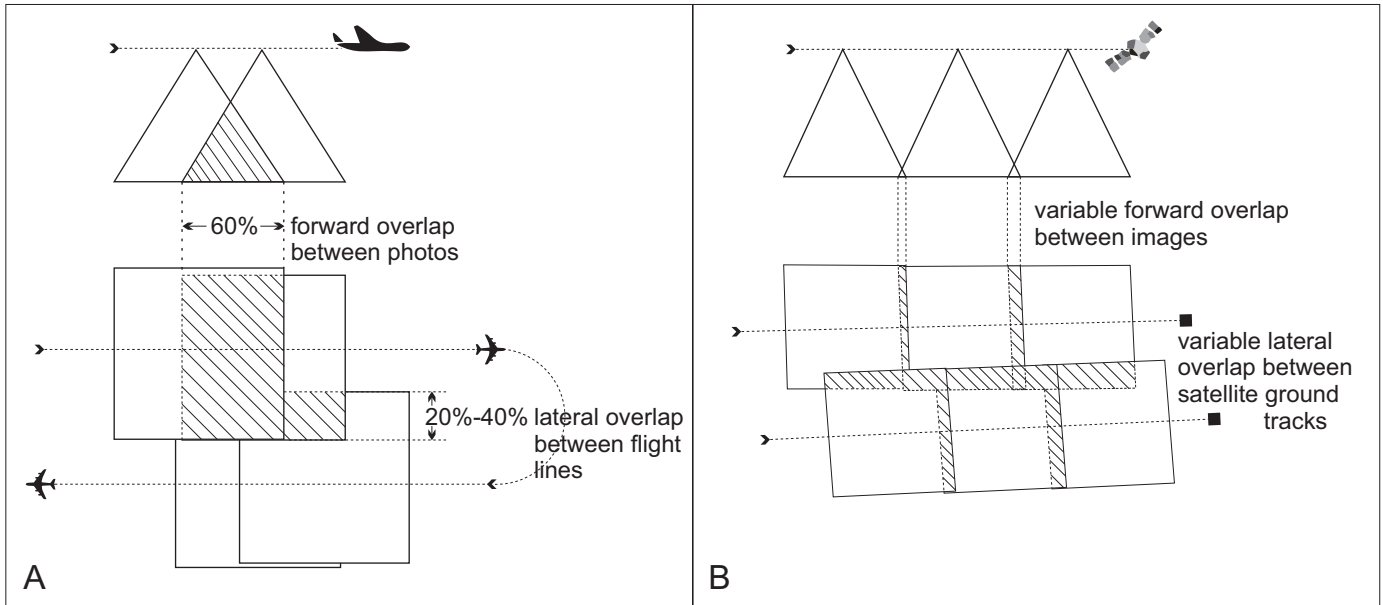


**Fig. 3. a)** Flight path for stereo imagery, with systematic overlap between sequential images. **b)** Flight path for non-stereo imagery, with variable overlap between sequential images. Modified after NRCAN (2016).

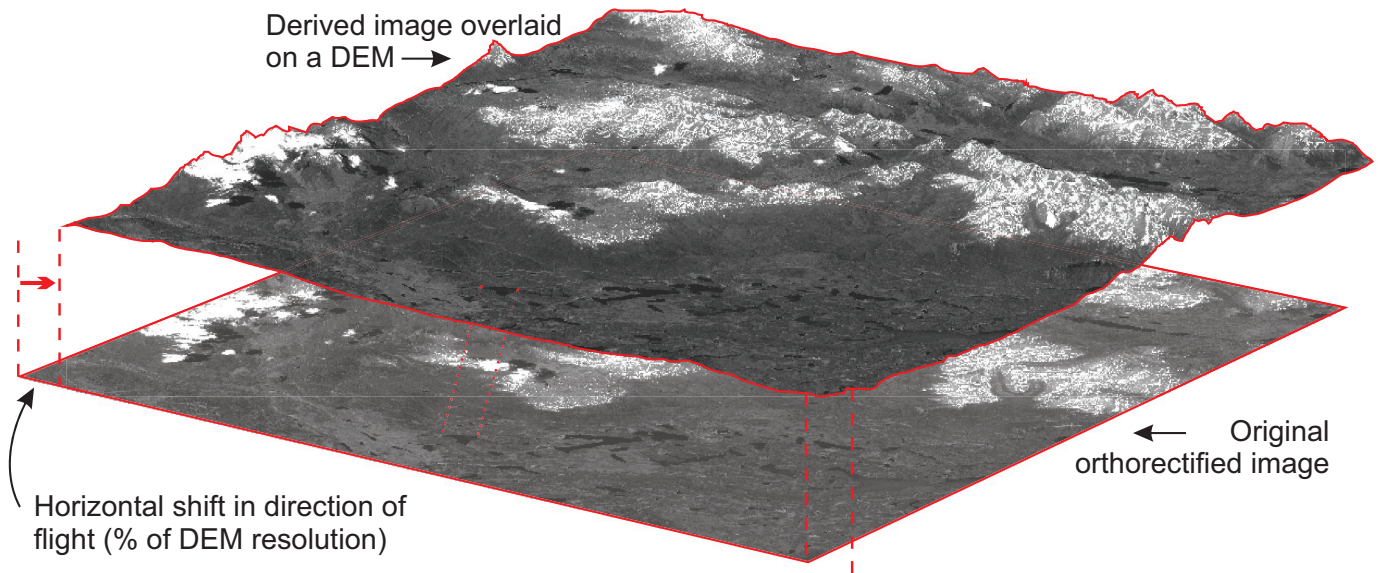


**Fig. 4.** Derived-stereo imagery is created by horizontally shifting a duplicate (derived image) in the flight direction. The derived image is then overlain on a DEM and georeferenced, providing a new perspective of the image based on topography. The amount of horizontal shift of the derived image is a percentage of the DEM resolution.

per frame. Each image covers about 130 km<sup>2</sup> with no overlap between images. The derived-stereo orthomosaic imagery was produced by a contractor for \$20 per image (Table 1).

### 3.3. Ice-flow mapping

We mapped ice-flow features for each imagery type, using Summit Evolution Lite running in tandem with ArcGIS, at scales of 1:4,000 (airphotos), 1:10,000 (SPOT imagery) and 1:4,000 (orthomosaics). Each feature was mapped manually

as a line (i.e., start node beginning up-ice and end node down-ice), recording length and directionality (unidirectional or bidirectional). Lines were converted to points and line azimuths were calculated and recorded. We then compared the data acquired from each imagery type. Where a feature was identified in different imagery types, we evaluated the consistency of location, length, azimuth, and if ice-flow directionality could be determined.

For the Atlin area, we compared features derived from:

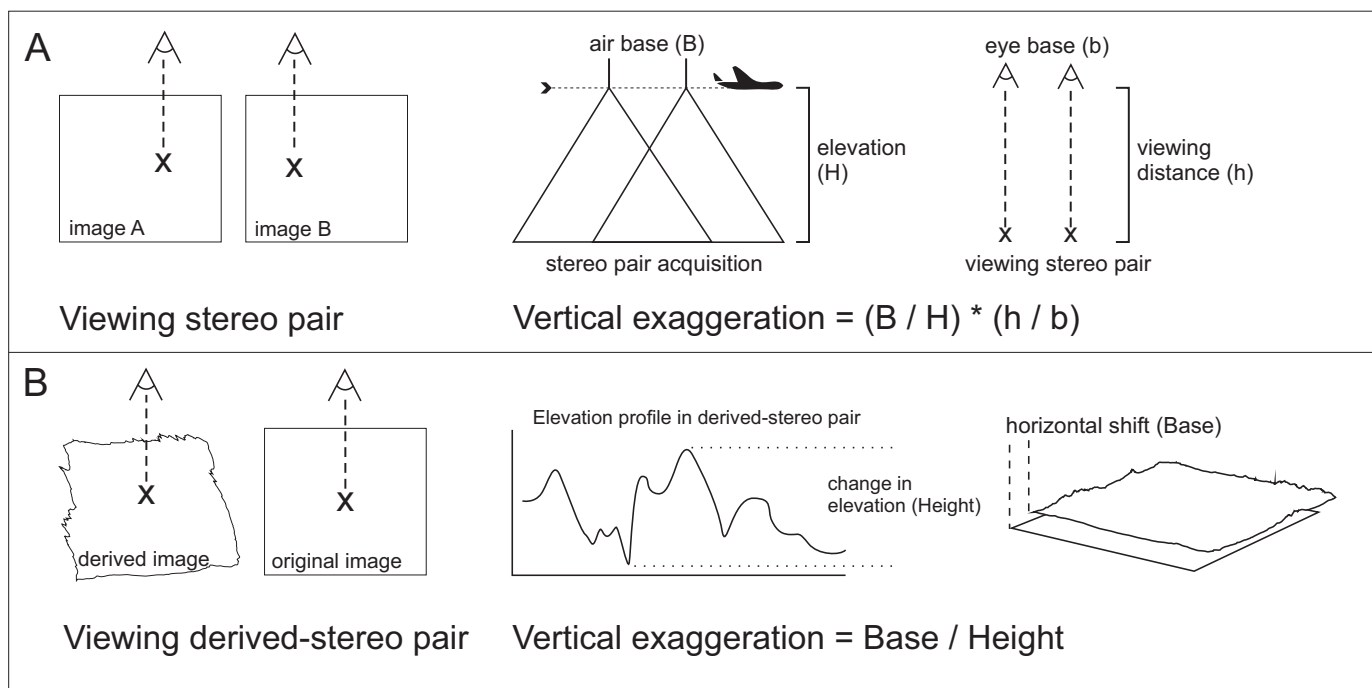


Fig. 5. Vertical exaggeration in a) Stereo imagery and b) Derived-stereo imagery. Modified from Sabins (1997) and Paine and Kiser (2012).

Table 1. Cost to create digital stereo and digital derived-stereo pairs for each imagery type.

Imagery type	Number of frames	Acquisition cost	Stereo/derived-stereo conversion (per frame)	Approximate area (km <sup>2</sup> )	Total		Cost per 100 km <sup>2</sup>
					cost	area (km <sup>2</sup> )	
Airphotos	59	\$ 18.50	\$ 20.00	68	\$ 2,271.50	4,000	\$ 56.79
SPOT	13	-	\$ 20.00	3,800	\$ 260.00	49,400	\$ 0.53
Orthomosaics	41	-	\$ 20.00	130	\$ 820.00	5,330	\$ 15.38

1) airphotos and mapping by Levson et al. (2003); 2) SPOT imagery and mapping by Levson et al. (2003); and 3) airphotos and SPOT imagery. For the Liard Plain area, we compared results from: 1) orthomosaic imagery and mapping by Gabrielse (1963); 2) SPOT imagery mapping by Gabrielse (1963); and 3) orthomosaic imagery and SPOT imagery.

Commonly, a single symbol is used to portray multiple streamlined features on surficial geology maps. Consequently, a single map symbol cannot be directly compared with a single ice-flow feature identified in the imagery. To enable more direct comparisons, we used buffers of 500 m and 1,000 m around each ice-flow map symbol in Levson et al. (2003) and Gabrielse (1963). In some cases ice-flow symbols in Levson et al. (2003) represent separations closer than 500 or 1000 m. In these situations, all ice-flow features in the imagery within 500 or 1,000 m of an ice-flow symbol were included in the comparison.

Levson et al. (2003) used hardcopy airphoto interpretation combined with field checks to produce earlier versions (see Levson, 1992; Levson and Kerr, 1992) of their map. Given that the same imagery type is used, significant differences

are unexpected when ice-flow features using digital airphotos are compared to those mapped by Levson et al. (2003). This comparison highlights the transition from hardcopy airphoto interpretation to the digital environment and provides a means of verifying the ice-flow features mapped using digital airphotos in part of the Atlin area (~780 km<sup>2</sup>). The methods used to produce Gabrielse (1963) map were not identified.

4. Results

4.1. Atlin area

4.1.1. Airphotos and features mapped by Levson et al. (2003)

Levson et al. (2003) shows 36 ice-flow symbols in an area of about 780 km<sup>2</sup> (Fig. 6; Table 2). Using the airphotos, 51 ice-flow features were identified in the same area. Of the ice-flow features recognized in the airphotos, 36 are within 500 m of 24 of the symbols in Levson et al. (2003). Therefore, within 500 m of where symbols were plotted, 12 of the ice-flow symbols in Levson et al. (2003) were not recognized on the airphotos (Fig. 7). Of the adjacent features, 47% on the airphotos have an ice-flow azimuth within 5° of the azimuth of the symbols

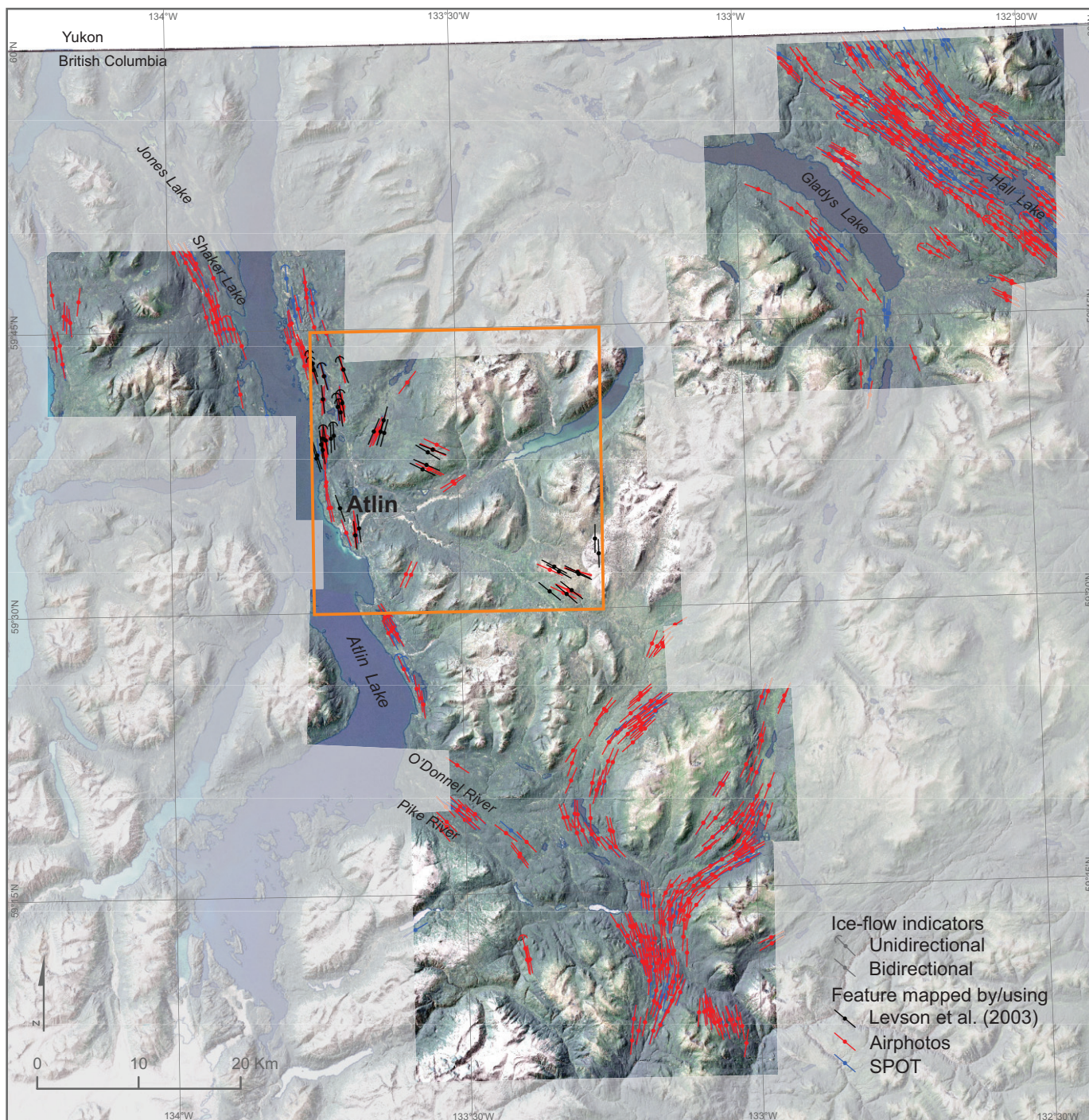


**Fig. 6.** Ice-flow feature mapping in the Atlin area. Orange box indicates area mapped by Levson et al. (2003).

on Levson et al. (2003) and 92% are within 10° (maximum discrepancy is 17°). The expanded 1,000 m buffer includes 42 ice-flow features identified in the airphotos. Thus, 33 of the 36 ice-flow symbols represented on the map have adjacent airphoto features within 1,000 m. Of the adjacent airphoto features, 43% have an ice-flow azimuth within 5° of symbols in Levson et al. (2003) and 83% are within 10° (maximum discrepancy of 18°; Table 3). Three ice-flow features identified by Levson et al. (2003) were not identified in the airphotos (Fig. 7, points

1-3). Two of these (Fig. 7, points 1-2) are in an area of high tonal saturation in the airphotos, which hampers identification. Levson et al. (2003) identified nine unidirectional features in the map area, but only one was identified in the airphotos, which underscores the importance of field checks.

**4.1.2. SPOT and features mapped by Levson et al. (2003)**

Using the SPOT imagery, 21 ice-flow features were identified in the area mapped by Levson et al. (2003). Of these, 17 are

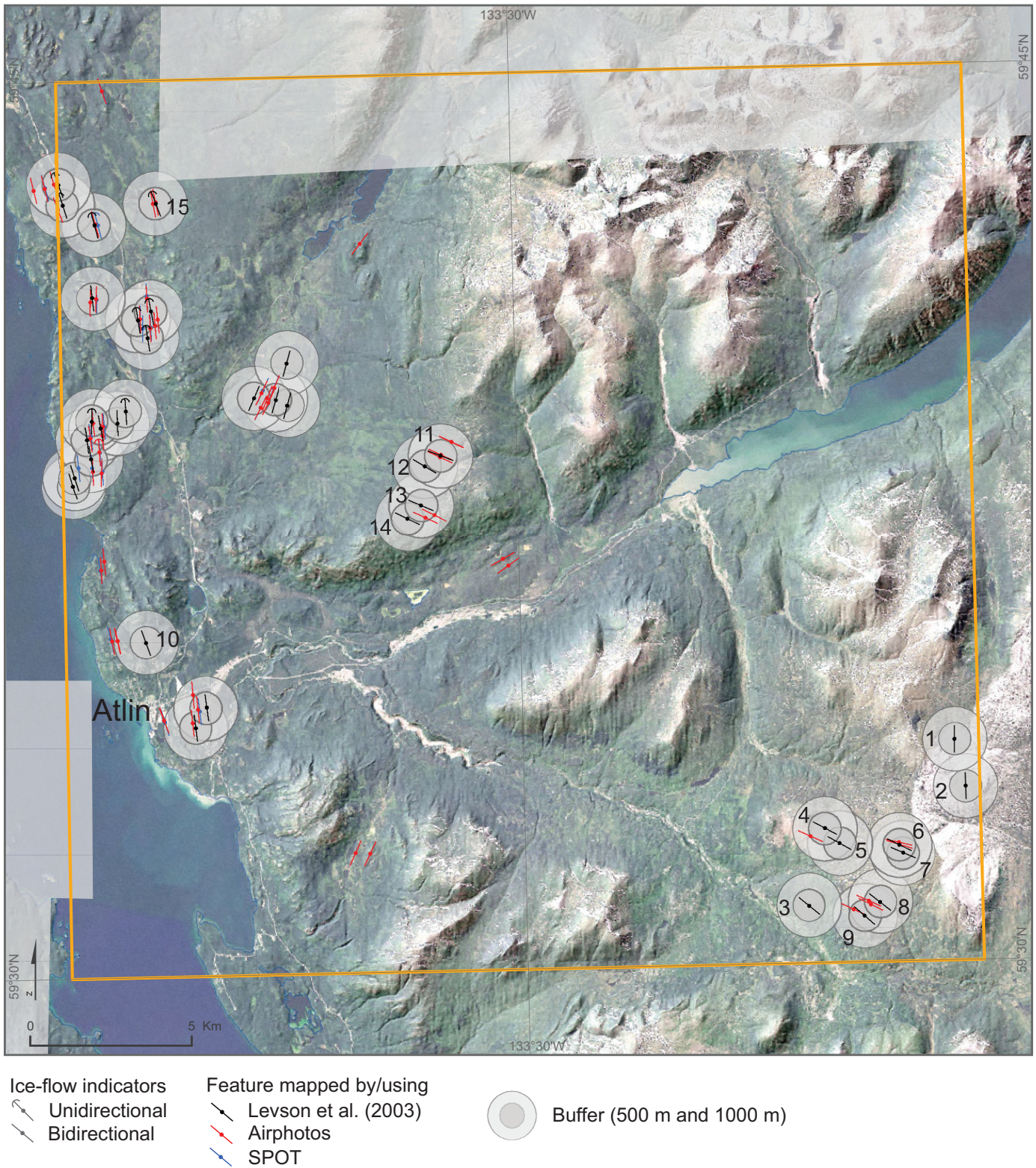


**Fig. 7.** Comparison of ice-flow mapping (orange box) completed by Levson et al. (2003) to features identified in airphotos and SPOT imagery. Two buffers of 500 m and 1,000 m were used. Numbers 1-3 depict features mapped by Levson et al. (2003) that were not identified in the airphotos. Numbers 1-15 depict features mapped by Levson et al. (2003) that were not identified in the SPOT imagery.

within 500 m of the ice-flow symbols in Levson et al. (2003). The 17 features are adjacent to 15 (of the 36) ice-flow symbols. Of these adjacent features, 35% of the ice-flow features from the SPOT imagery have an azimuth within 5° of the mapped symbols, and 94% are within 10° (maximum discrepancy of 12°). A total of 18 ice-flow features identified using SPOT imagery are within 1,000 m of the symbols on Levson et al. (2003). The 18 SPOT features are adjacent to 21 of the 36 ice-flow symbols in Levson et al. (2003). Of the SPOT ice-flow features, 28% have an azimuth within 5° of the symbols on the map and 72% are within 10° (maximum difference of 15°; Table 3). Fifteen of the 36 features symbolized in Levson et al. (2003) lacked corresponding features in the SPOT imagery (Fig. 7, points 1-15). One unidirectional ice-flow feature was identified in the SPOT imagery that is within 500 m of a unidirectional feature identified by Levson et al. (2003).

**4.1.3. Airphotos and SPOT imagery**

In the area of overlapping airphoto and SPOT imagery (about 4,000 km<sup>2</sup>), 579 ice-flow features were detected using airphotos; 35 were identified as unidirectional (Table 2). Using the SPOT

imagery, 349 ice-flow features were identified, nine of which are unidirectional (Table 2). Comparing the airphoto and SPOT imagery datasets, 249 of the ice-flow features are coincident in both imagery types (Figs. 6, 8). Several longer ice-flow features identified in the SPOT imagery appear as two separate features in the airphotos. In some cases, parallel features in the airphotos appear as a single feature in the SPOT imagery. Variance in the ice-flow direction of the features identified in the two imagery types is low; 91% of coincident features have azimuths within 5° (Table 3) and the largest discrepancy is 11°. The median difference in the length of a feature mapped using both imagery types is 119 m. However, the features were not longer consistently in one imagery type. Only one feature was mapped as unidirectional in both the airphotos and SPOT imagery.

**4.2. Liard Plain area**

**4.2.1. Orthomosaic imagery and features mapped by Gabrielse (1963)**

The Gabrielse (1963) map overlaps with the western half of the Liard Plain area. Gabrielse (1963) mapped 19 ice-flow features

**Table 2.** Ice-flow features identified in imagery types.

Map area	Ice-flow feature mapping	Total number of features	Unidirectional features
Atlin	Airphoto	579	35
	SPOT	349	9
	Single feature identified in airphoto & SPOT	249	1
	Levson et al. (2003)	36	9
Liard Plain	Orthomosaics	741	41
	SPOT	275	10
	Single feature identified in orthomosaic & SPOT	154	0
	Gabrielse (1963)	19	19

**Table 3.** Variability of ice-flow direction in features identified in two imagery types and each imagery type to published maps.

Map area	Ice-flow feature mapping	Ice-flow direction variance			Median absolute difference in length (m)	
		Buffer	within 5°	within 10°		max
Atlin	Airphoto & SPOT		91%	99.60%	11	119
	Levson et al. (2003) & airphoto	500 m	47%	92%	17	
		1000 m	43%	83%	18	
	Levson et al. (2003) & SPOT	500 m	35%	94%	12	
1000 m		28%	72%	15		
Liard Plain	Orthomosaic & SPOT		92%	100%	8	117
	Gabrielse (1963) & orthomosaic	500 m	64%	91%	11	
		1000 m	60%	86%	17	
	Gabrielse (1963) & SPOT	500 m	100%	100%	2	
1000 m		87%	100%	7		

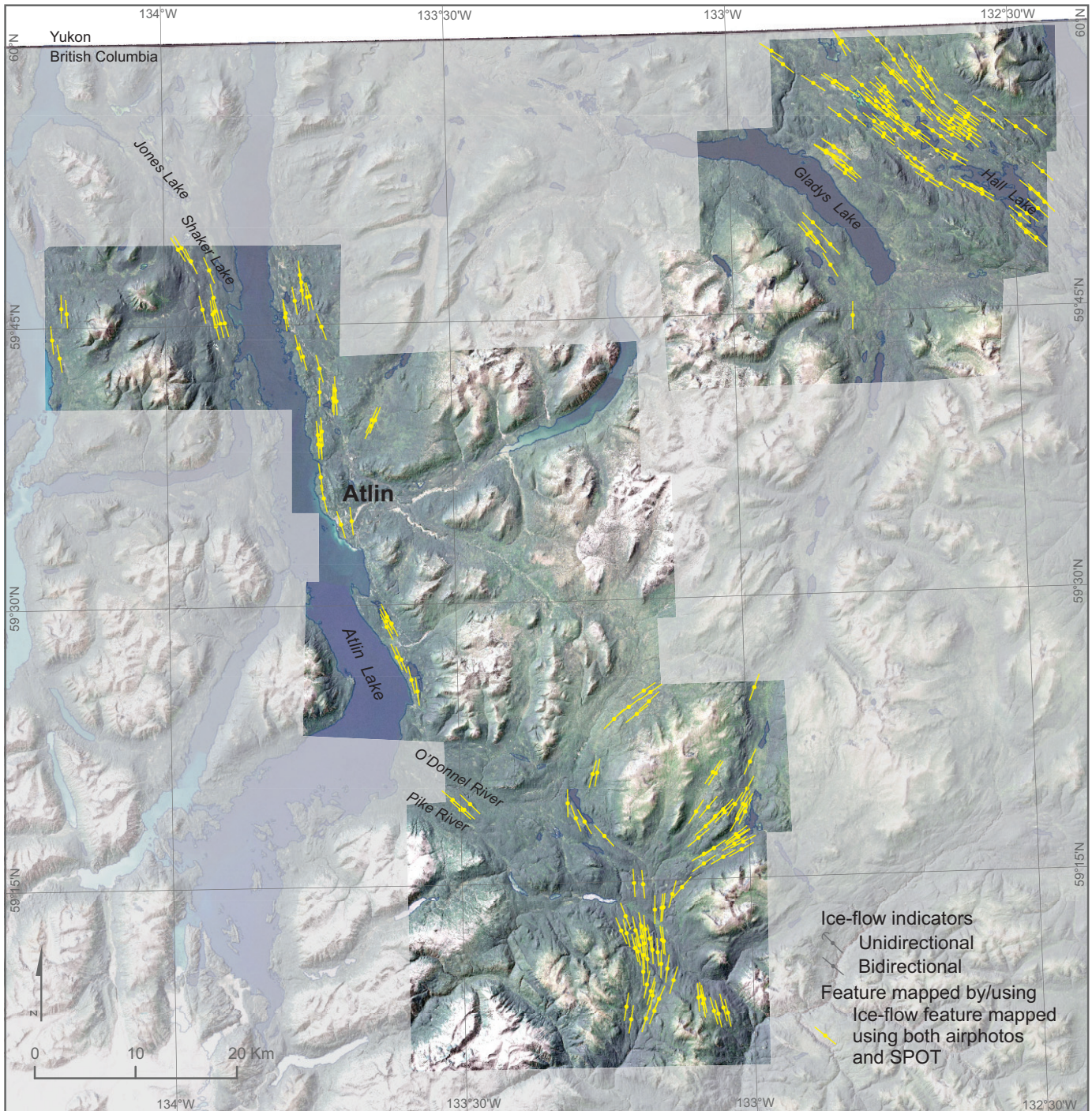


**Fig. 8.** Ice-flow features identified in both airphotos and SPOT imagery in the Atlin area.

in an area of about 2,020 km<sup>2</sup> (Fig. 9; Table 2). In the same area, 393 ice-flow features were identified in the orthomosaics. Eleven features identified using orthomosaics are within 500 m of eight of the 19 features in Gabrielse (1963). Eleven of the features symbolized on the Gabrielse (1963) map were not identified within 500 m in the orthomosaics. Of the Gabrielse (1963) symbols within 500 m, 64% of the orthomosaic features have an ice flow direction within 5°, and 91% are within 10°

(with maximum discrepancy of 11°). When comparing the ice-flow features identified in the orthomosaics to the symbols in the Gabrielse (1963) map using the 1,000 m buffer, 49 features identified using orthomosaics are within 1,000 m of 13 of the 19 ice-flow features symbolized by Gabrielse (1963). Of the adjacent features, 60% of the orthomosaic features have an azimuth within 5° of the symbolized features in Gabrielse (1963) and 86% are within 10° (maximum discrepancy of 17°;

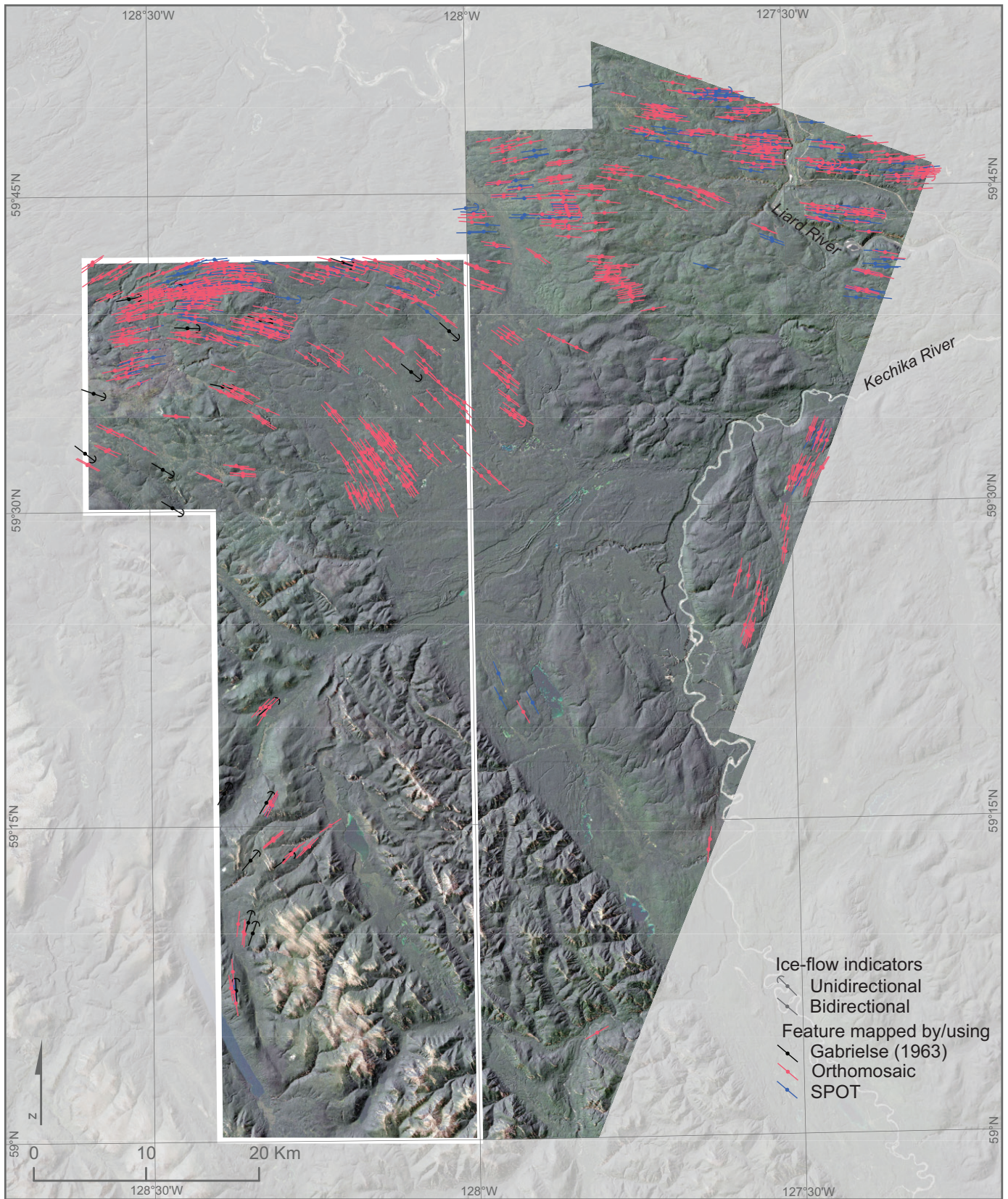


Fig. 9. Ice-flow features mapped in the Liard Plain area. Gabrielse (1963) map outlined in white.

Table 3). Six ice-flow features symbolized by Gabrielse (1963) were not identified in the orthomosaic (Fig. 10, points 1-6). All of the 19 features symbolized in Gabrielse (1963) indicate unidirectional flow. Of the 19 unidirectional features identified in the orthomosaics, only two are within 1,000 m of those symbolized by Gabrielse (1963).

#### 4.2.2. SPOT and features mapped by Gabrielse (1963)

Using the SPOT imagery, 94 ice-flow features were identified in the area mapped by Gabrielse (1963). Three features are immediately adjacent to two symbols on the Gabrielse (1963) map and have ice-flow directions within 5°. The SPOT imagery identified 15 ice-flow features within 1,000 m of six features symbolized by Gabrielse (1963). Of the adjacent SPOT ice-flow features, 87% have ice-flow directions within 5° of the symbolized features and all are within 10° (maximum discrepancy of 7°; Table 3). Thirteen symbols in the Gabrielse (1963) map were not identified using SPOT (Fig. 10, points 1-13). One unidirectional ice-flow feature was identified in the SPOT imagery, and it is within 1,000 m of a unidirectional symbol in Gabrielse (1963).

#### 4.2.3. Orthomosaic imagery and SPOT imagery

In the area with overlapping orthomosaic and SPOT imagery (approximately 4,450 km<sup>2</sup>), 741 ice-flow features were identified using orthomosaics, of which 41 are unidirectional. A total of 257 ice-flow features are identified using the SPOT imagery, of which 10 are unidirectional. In this overlap area, 154 ice-flow features coincide (Figs. 9, 11; Table 2). Several features identified as single features in the SPOT imagery appear as two separate features in the orthomosaics. In the orthomosaics, some appear as two shorter features with the same bearing, with the centreline of pairs coinciding with the feature mapped in the SPOT imagery. Variance in ice-flow directions of the coincident features identified in the two imagery types is low, as 92% of the features are within or below 5°, with a maximum discrepancy of 8° (Table 3). The median difference in length of a feature mapped using both imagery types is 117 m; 60% of coincident occurrences are longer in the orthomosaics. Three features were mapped as unidirectional in both imagery types.

### 5. Discussion

Consistencies between datasets indicate that derived-stereo imagery is useful for remotely generating macroscale ice-flow data for inclusion in regional compilations. Comparison of data from the Atlin area suggests that digital stereoscopic airphoto imagery, which has the highest spatial resolution, is the most effective. Although fewer ice-flow features are resolved in the SPOT data, major flow sets are discernible and the number of features mapped is adequate to determine a general ice flow history. Data comparison in the Liard Plain reveals that orthomosaics may be superior to SPOT, again reflecting better resolution of the imagery.

Airphotos are the traditional and proven method for mapping landforms (e.g., Mollard, 1976). Because ice flow-sets are often

depicted on maps as a symbol, direct comparison of ice-flow features identified in stereoscopic airphotos and those depicted by map symbols is limited. Two clusters of ice-flow features depicted on the Levson et al. (2003) map were not detected with the stereoscopic airphotos. These features may have been encountered during fieldwork (Fig. 7, points 1 and 2, and 3). Five clusters of ice-flow features depicted in the Levson et al. (2003) map were not detected in the SPOT data. Nevertheless, most of the major flow sets are clearly identified by the SPOT data (Fig. 7).

However, our evaluation suggests that most of the major flow sets identified in Levson et al. (2003) are recognizable by using the stereoscopic airphotos to map ice-flow features. Furthermore, there is limited variation in the flow azimuths between the stereoscopic airphotos datasets and the symbols depicted on the maps. In the Atlin area 40% fewer features were recognized in SPOT images (n=349) than in the airphotos (n=579). Some subtle features (e.g., points 4-9, 11-14, Fig. 7) were detected in the stereoscopic airphotos but not in the SPOT images.

The derived-stereo has a number of limitations. Whereas ice-flow direction is consistent in all the datasets, unidirectional features, mapping density, and spatial distribution differ. Each imagery type differs in imagery resolution, cloud cover, and light saturation/desaturation, which may lead to mapping inconsistencies. More ice-flow features were mapped and more unidirectional ice-flow features identified using higher resolution imagery. Cloud cover affected mapping using SPOT imagery, because one derived-stereo pair was completely obscured. Cloud cover was not a factor when using orthomosaics because the images selected are cloud free. Airphotos and SPOT images have areas of high and low tonal saturation, which reduces the ability to identify ice-flow features. This is not an issue with the orthomosaics because they have a consistent tonal range (white to black).

The derived-stereo pairs were produced with the same horizontal offset across imagery and terrain types. This produced variation in vertical exaggeration between derived-stereo pairs (Fig. 5). This may be a factor in the mapping distribution, density, and identification of unidirectional features. For example, SPOT images have a large spatial footprint compared to orthomosaics (Table 1). Due to the larger spatial footprint, difference in relief across a SPOT image is larger, creating a greater vertical exaggeration than in the overlapping multiple orthomosaics. This causes the same feature across imagery types to look different and, therefore, be mapped differently. Our evaluation indicates that most of the ice-flow sets symbolized in Gabrielse (1963) are recognizable using orthomosaics.

The cost of mapping using stereo derived imagery is a significantly less than traditional hardcopy airphoto mapping and digital stereo airphoto mapping (Table 1). Although there are cost savings through efficiencies gained through mapping in digitally, (e.g., Smith et al., 2011), digital stereo airphotos of large areas is still expensive. Orthomosaic derived imagery

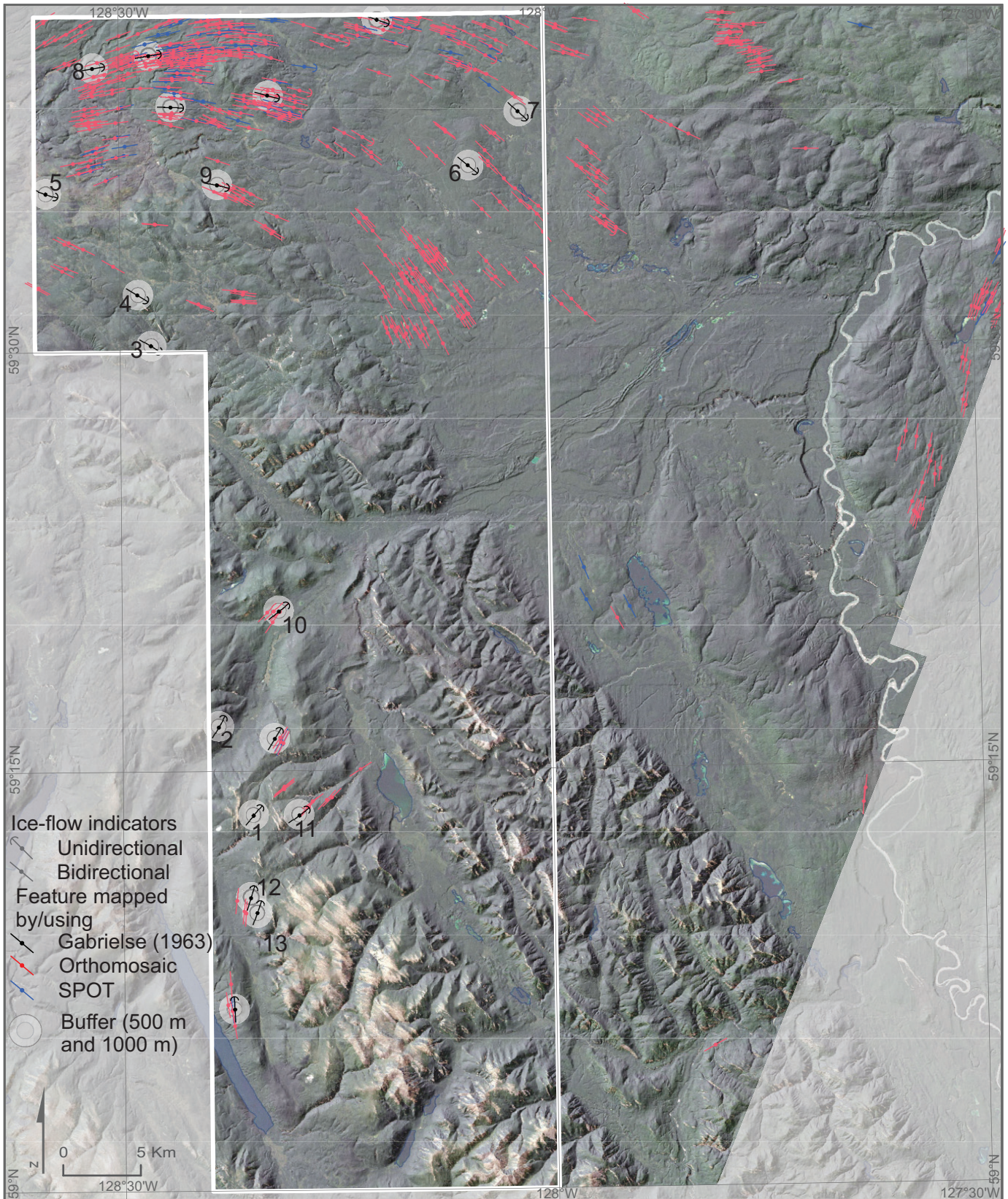


**Fig. 10.** Comparison of ice-flow mapping completed by Gabrielse (1963), outlined in white, to features identified in orthomosaics and SPOT imagery. Two buffers of 500 m and 1,000 m were used. Numbers 1-6 depict features mapped by Gabrielse (1963) that were not identified in the orthomosaics. Numbers 1-13 depict features mapped by Gabrielse (1963) that were not identified in the SPOT imagery.

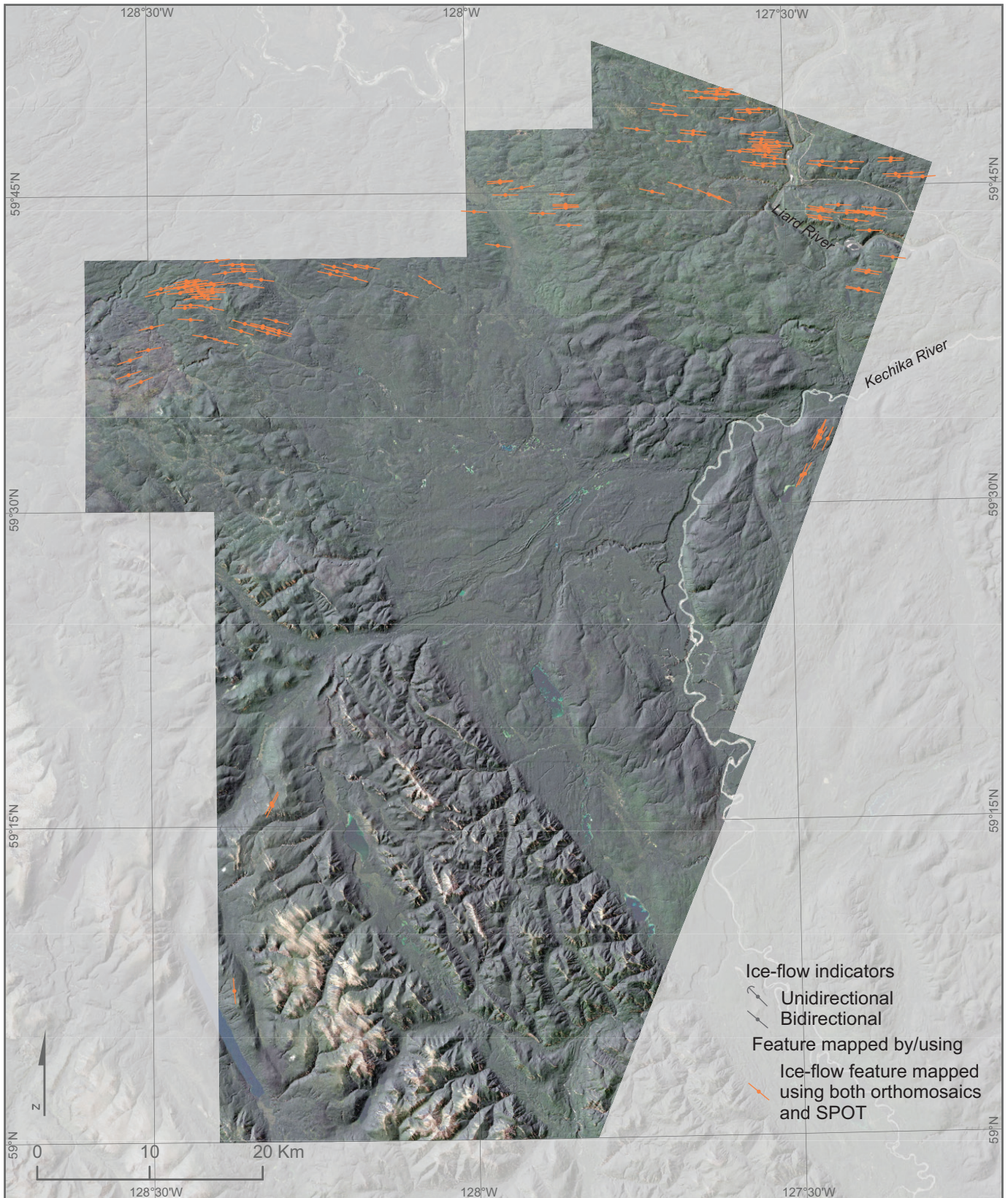


Fig. 11. Ice-flow features identified in both orthomosaics and SPOT imagery in the Liard Plain area.

costs 27% less than digital stereo airphoto derived imagery, with minimal loss in the accuracy and density of ice-flow features. The cost of SPOT derived-stereo imagery is less than 1% of the digital stereo airphoto and less than 3% of the orthomosaic derived-stereo imagery. Although the loss of fidelity is significant, the loss is at the regional scale and SPOT derived-stereo imagery highlight the most significant ice-flow sets. We conclude that, for mapping regional macroscale ice-flow features, the derived-stereo orthomosaic imagery balances accuracy with cost and provides the best value, but only for agencies within the British Columbia government. Outside of government, each orthomosaic frame has a maximum cost of about \$200, which equates to \$169/100 km<sup>2</sup>, making this dataset the most expensive.

## 6. Conclusions

Derived-stereo imagery provides the ability to incorporate single-frame imagery types into traditional stereo mapping methods at a significantly less cost than traditional hardcopy airphoto mapping and digital stereo airphoto mapping. Our evaluation indicates that derived-stereo orthomosaics provide the best value to remotely map ice-flow features, but only for government agencies that can access imagery at no cost. This evaluation was completed as part of the British Columbia Geological Survey's ice-flow indicator compilation for British Columbia and Yukon and might be useful to others. Ice-flow features mapped using derived-stereo SPOT imagery is inexpensive and has merit for regional ice-flow studies, but is inferior to digital stereo airphotos and derived-stereo orthomosaics.

## Acknowledgments

This project was partly funded by the Geological Survey of Canada Geo-mapping for Energy and Minerals phase 2 (GEM 2) program. We thank Ian Grady (iGi Consulting, Port Coquitlam, BC) for producing the derived-stereo imagery and appreciate the valuable input provided by Yao Cui (British Columbia Geological Survey). We also thank Daniel Kerr (Geological Survey of Canada) and the Geological Survey of Canada for their partnership and financial support.

## References cited

- Aber, J.S., Marzloff, I., and Ries, J.B., 2010. Small-format aerial photography: Principles, techniques and geoscience applications. Elsevier, The Netherlands, 265 p.
- Arnold, H., Ferbey, T., and Hickin, A.S., 2016. Ice-flow indicator compilation, British Columbia and Yukon. British Columbia Ministry of Energy and Mines, British Columbia Geological Survey Open File 2016-04; Geological Survey of Canada, Open File 8083, 1:1,750,000 scale.
- Aitken, J.D., 1959. Atlin area, British Columbia. Geological Survey of Canada Memoir 307, 89 p.
- Bednarski, J.M., 2008. Landform assemblage produced by the Laurentide Ice Sheet in northeast British Columbia and adjacent Northwest Territories – constraints on glacial lakes and patterns of ice retreat. *Canadian Journal of Earth Sciences* 45, 593-610.
- Benn, D.I., and Evans, D.J.A., 2010. *Glaciers and Glaciations*. Second Edition. Arnold, London, pp. 259-579.
- Boulton, G.S., 1987. A theory of drumlin formation by subglacial sediment deformation. In: Menzies, J., Rose, J. (Eds.), *Drumlin Symposium*. Balkema, Rotterdam, 25–80.
- Boulton G.S., Dongelmans, P., Punkari, M., and Broadgate, M., 2001. Palaeoglaciology of an ice sheet through a glacial cycle: the European ice sheet through the Weichselian. *Quaternary Science Reviews* 20, 591-625.
- Clague, J.J., 1989. Chapter 1: Quaternary geology of the Canadian Cordillera; in *Quaternary Geology of Canada and Greenland*. In: Fulton, R.J. (Ed.), *Geology of Canada Series No. 1.*, 17-96.
- Clague, J.J., and Ward, B., 2011. Pleistocene Glaciation of British Columbia. In: Ehlers, J., Gibbard, P.L., Huges, P.D., (Eds.), *Quaternary glaciations- extent and chronology, a closer look*. *Developments in Quaternary Science* 15, 563-573.
- Clark, C.D., 1993. Mega-scale lineations and cross-cutting ice-flow landforms. *Earth Surface Processes and Landforms* 18, 1–29.
- Clark C.D., Hughes, A.L.C., Greenwood, S.L., Jordan, C., and Sejrup, H.P., 2012. Pattern and timing of retreat of the last British-Irish ice sheet. *Quaternary Science Reviews* 44, 112-144.
- DATEM, 2012. Summit Evolution Operation Manual edition 6.4. DAT/EM Systems International, pp “4-11”.
- Evans, D.J.A., Rea, B.R., Hiemstra, J.F., and Ó Cofaigh, C., 2006. A critical assessment of subglacial mega-floods: A case study of glacial sediments and landforms in south-central Alberta, Canada. *Quaternary Science Reviews* 25 (13-14), 1638-1667.
- Ferbey, T., and Arnold, H., 2013. Compilation of micro- to macroscale ice-flow indicators for the Interior Plateau, central British Columbia. British Columbia Ministry of Energy, Mines and Natural Gas, British Columbia Geological Survey, Open File 2013-03, 1:900,000 scale.
- Ferbey, T., Arnold, H., and Hickin, A.S., 2013. Ice-flow indicator compilation, British Columbia. British Columbia Ministry of Energy, Mines and Natural Gas, British Columbia Geological Survey Open File 2013-06, 1:1 650,000 scale.
- Fulton, R.J., 1991. A conceptual model for growth and decay of the Cordilleran Ice Sheet. In: *Géographie physique et Quaternaire* 45, 281-286.
- Gabrielse, H., 1963. McDame map-area, Cassiar District, British Columbia. Geological Survey of Canada Memoir 319, 138 p.
- Holland, S.S., 1976. Landforms of British Columbia; a physiographic outline. British Columbia Ministry of Energy and Mines, British Columbia Geological Survey Bulletin 48, 138 p.
- Huntley, D.H., Hickin, A.S., and Lian, O.B., 2016. The pattern and style of deglaciation at the Late Wisconsinan Laurentide and Cordilleran ice sheet limits in northeastern British Columbia. *Canadian Journal of Earth Sciences*, doi:10.1139/cjes-2016-0066.
- Jackson, L.E., Jr., 1994. Terrain inventory and Quaternary history of the Pelly River area, Yukon Territory. Geological Survey of Canada Memoir 437, 41 p.
- Jackson L.E., Jr., and Clague, J.J. (Eds), 1991. The Cordilleran Ice Sheet. In: *Géographie physique et Quaternaire* 45, 261–377.
- Jackson, L.E., Jr. and Mackay, T.D., 1990. Glacial limits and ice flow directions for the last Cordilleran Ice Sheet in Yukon Territory between 60 and 63 degrees north. Geological Survey Open File 2329, 1 sheet, doi:10.4095/131319.
- Jackson, L.E., Jr., Ward, B., Duk-Rodkin, A., and Hughes, O.L., 1991. The last Cordilleran Ice Sheet in southern Yukon Territory. *Géographie Physique et Quaternaire*, 45, 341-354.
- Kennedy, K.E., and Bond, J.D., 2004. Evidence for a late-McConnell readvance of the Cassiar Lobe in Seagull Creek, Pelly Mountains, Central Yukon. In: Emond, D.S., and Lewis, L.L. (Eds), *Yukon exploration and geology 2003*, 121-128.
- King, E.C., Hindmarsh, R.C.A., and Stokes, C.R., 2009. Formation of mega-scale glacial lineations observed beneath a West Antarctic ice stream. *Nature Geoscience* 2, 585-588.
- Kleman, J., Hätteland, C., Borgström, I., and Stroeven, A., 1997. Fennoscandian palaeoglaciology using a glacial geological

- inversion model, *Journal of Glaciology* 43, 283-299.
- Landgrebe, D.A., 2003. Signal theory methods in multispectral remote sensing. Wiley and Sons Inc., New Jersey, 508p.
- Levson, V.M., 1992. Quaternary geology of the Atlin area (104N/11W, 12 E). In: *Geological Fieldwork 1991*. British Columbia Ministry of Energy, Mines and Petroleum Resources, British Columbia Geological Survey Paper 1992-1, pp. 375-390.
- Levson, V.M., and Kerr, D.E., 1992. Surficial geology and placer gold setting of the Atlin – Surprise Lake area, NTS 104/11, 12. British Columbia Ministry of Energy, Mines and Petroleum Resources, British Columbia Geological Survey Open File 1992-7, 1:50,000 scale.
- Levson, V.M., Kerr, D.E., Lowe, C., and Blyth, H., 2003. Quaternary geology of the Atlin area, British Columbia. British Columbia Ministry of Energy and Mines, British Columbia Geological Survey Geoscience Map 2003-1; Geological Survey of Canada Open File 1562, 1:50,000 scale.
- Margold, M., Jansson, K.N., Kleman, J., and Stroven, A.P., 2013. Lateglacial ice dynamics of the Cordilleran Ice Sheet in northern British Columbia and southern Yukon Territory: retreat pattern of the Liard Lobe reconstructed from the glacial landform record. *Journal of Quaternary Science* 28 (2), 180-188.
- Menzies, J., 1979. A review of the literature on the formation and location of drumlins. *Earth Science Reviews* 14, 315-359.
- Mollard, J.D., 1976. Landforms and surface materials of Canada – A Stereoscopic airphoto atlas and glossary. Eighth edition. Regina, Saskatchewan, 171p.
- NRCAN, 2016. Concepts of Aerial Photography. Downloaded from <http://www.nrcan.gc.ca/earth-sciences/geomatics/satellite-imagery-air-photos/air-photos/about-aerial-photography/9687> [accessed October, 2016].
- Paine, D.P., and Kiser, J.D., 2012. Aerial photography and image interpretation. Third edition. Wiley, Hoboken, New Jersey, USA, 56.
- Ryder, J.M., and Maynard, D., 1991. The Cordilleran Ice Sheet in northern British Columbia. *Géographie Physique et Quaternaire* 45, 355-363.
- Sabins, F.F., 1997. Remote sensing: principles and applications. Third edition. Waveland Press Inc., Long Grove, Illinois, USA, 45.
- Seguinot, J., Rogozhina, I., Stroeven, A.P., Margold, M., and Kleman, J., 2016. Numerical simulations of the Cordilleran ice sheet through the last glacial cycle. *Cryosphere* 10, 639-664.
- Smith, M.J., Paron, P., Griffiths, J.S. (eds), 2011. *Geomorphological mapping, methods and applications*. Elsevier, 611p.
- Spagnolo, M., Clark, C.D., Ely, J.C., Stokes, C.R., Anderson, J.B., Andreassen, K., Graham, A.G.C., and King, E.C., 2014. Size, shape and spatial arrangement of mega-scale glacial lineations from a large and diverse dataset. *Earth Surface Processes and Landforms* 39, 1432-1448.
- SPOT (SPOT 4 and SPOT 5 satellite imagery), 2010. Downloaded from <http://www.geobase.ca> (November 2014).
- SRTM (Shuttle Radar Topography Mission 1 Arc-second Global). 2014. Downloaded from <https://lta.cru.usgs.gov/SRTM1Arc> [November 2014].
- Stokes, C.R., Tarasov, L., Blomdin, R., Cronin, T.M., Fischer, T.G., Gyllencreutz, R., Hättstrand, C., Heyman, J., Hindmarsh, R.C.A., Hughes, A.L.C., Jakobsson, M., Kirchner, N., Livingstone, S.J., Margold, M., Murton, J.B., Noormets, R., Peltier, W.R., Peteet, D.M., Piper, D.J.W., Preusser, F., Renssen, H., Roberts, D.H., Roche, D.M., Saint-Ange, R., Stroven, A.P., and Teller, J.T., 2015. On the reconstructions of paleo-ice sheets: Recent advances and future challenges. *Quaternary Science Reviews* 125, 15-49.
- Stumpf, A.J., Broster, B.E., and Levson, V.M., 2000. Multiphase flow of the late Wisconsinan Cordilleran ice sheet in western Canada. *Geological Society of America Bulletin* 112, 1850-1863.